Author(s): Haaranen, Mikko; Kotila, Jenni-Mari; Suhonen, Jouni

Title: Spectrum-shape method and the next-to-leading-order terms of the β-decay shape factor

Year: 2017

Version:

Please cite the original version:

Haaranen, M., Kotila, J.-M., & Suhonen, J. (2017). Spectrum-shape method and the next-to-leading-order terms of the β-decay shape factor. Physical Review C, 95(2), Article 024327. https://doi.org/10.1103/PhysRevC.95.024327

Spectrum-shape method and the next-to-leading-order terms of the β-decay shape factor

M. Haaranen, J. Kotila, and J. Suhonen
Department of Physics, University of Jyväskylä, P.O. Box 35 (YFL), FI-40014 Jyväskylä, Finland
(Received 10 November 2016; published 28 February 2017)

Effective values of the axial-vector coupling constant g_A have lately attracted much attention due to the prominent role of g_A in determining the half-lives of double β decays, in particular their neutrinoless mode. The half-life method, i.e., comparing the calculated half-lives to the corresponding experimental ones, is the most widely used method to access the effective values of g_A. The present paper investigates the possibilities offered by a complementary method: the spectrum-shape method (SSM). In the SSM, comparison of the shapes of the calculated and measured β electron spectra of forbidden nonunique β decays yields information on the magnitude of g_A. In parallel, we investigate the impact of the next-to-leading-order terms of the β-decay shape function and the radiative corrections on the half-life method and the SSM by analyzing the fourfold forbidden decays of ^{113}Cd and ^{115}In by using three nuclear-structure theory frameworks; namely, the nuclear shell model, the microscopic interacting boson-fermion model, and the microscopic quasiparticle-phonon model. The three models yield a consistent result, $g_A \approx 0.92$, when the SSM is applied to the decay of ^{113}Cd for which β-spectrum data are available. At the same time the half-life method yields results which are in tension with each other and the SSM result.

DOI: 10.1103/PhysRevC.95.024327

I. INTRODUCTION

The general features of the nuclear single β decay are well established and fairly extensively tested throughout the nuclear landscape [1,2]. The recent developments in the field of β decay have led to the application of the theoretical formalism to the more extreme types of β decay. Typically these are transitions characterized by extensively long partial half-lives and in many cases they are masked by the competing faster decay channels. The retardation of these rare types of single β decay typically results from the following conditions: (a) the required angular-momentum change between the initial and final nuclear state is large, and/or (b) the transition Q value (energy available for the decay) is low ($<$100 keV). Examples of such studies include up to sixfold forbidden β transitions, and those of ultralow Q values (see, e.g., Refs. [3–9]).

Aside from the theoretical and experimental development leading to the studies of the rare β decays, another point of interest has been the problem concerning the effective values of the weak coupling constants. Initially, the two coupling constants, i.e., the vector coupling constant g_V and the axial-vector coupling constant g_A, enter the β-decay theory as means of renormalizing the hadronic current. The "bare" or "canonical" values of $g_V = 1.0$ and $g_A = 1.27$ [10] stem from the conserved vector current (CVC) hypothesis and partially conserved axial-vector current (PCAC) hypothesis [11]. Corrections to these bare values can stem from, e.g., the non-nucleonic degrees of freedom [12,13], but in the context of practical nuclear-structure calculations additional shortcomings of the many-body treatment can also be absorbed into these constants. These shortcomings stem from the nuclear many-body effects that include the truncations in the model space and/or deficiencies in handling the many-body quantum mechanics [14,15].

As mentioned earlier, the canonical free-nucleon values of the weak constants are fixed by considerations of the electroweak theory. Although both of the weak constants might be subject to quenching (see, e.g., Refs. [16–19] for the discussion on the effective values of g_V), the particular interest in the effective values of g_A is explained by the studies made on the neutrinoless double β decay. The decay rate of this mode is proportional to g_A^4 [20,21], and thus any uncertainties related to the values of the axial-vector coupling pose a substantial difficulty when considering the experimental verification of this decay branch (see, e.g., Refs. [22,23]).

Up until recently the usual analyses on the effective values of weak coupling constants have been revolving around the computation of the single-β-decay and double-β-decay (the two-neutrino mode) partial half-lives. The effective values of the axial-vector coupling constant are extracted when a reasonable match with experiment is found by fine tuning the value of g_A. These studies have been performed in the context of the proton-neutron quasiparticle random-phase approximation (pnQRPA) [14,15,22–26], the nuclear shell model (NSM) [27–29], and the interacting boson model (IBM) [30–32]. The general trends seem to suggest a need for a fairly strong quenching of g_A. In most of these studies effective values of less than unity appear.

To access a complementary way of getting insight into the problem of the coupling constants, a new method, called the spectrum-shape method (SSM) was introduced in Ref. [8]. Instead of drawing the conclusions solely from the partial half-lives, the spectra of the emitted β particle, i.e., the β spectra, can also be used to aid the search. The proposed method is based on the observation that the many nuclear matrix elements (NMEs) of the forbidden nonunique β^--decay branches can make the shape of the β spectra strongly depend on the chosen values of the weak coupling constants. Suitable values of these constant can then be found by performing a comparison between the theoretical and the experimental β spectra.

All (but one, Ref. [8]) of the previous studies on single β decay restrict the inspection of the partial half-lives to the leading-order terms of the β-decay shape factor (see, e.g., Refs. [5–7]). Likewise, many of the other higher-order

corrections are typically neglected. In the current article we want to extend the presentation of Ref. [8] by gathering the theoretical formalism compactly under one heading. More notably we want to concentrate on the extension of the β-decay theory to the next-to-leading order following the discussion in Refs. [1,2]. Although the major part of the theory is well contained in the lowest-order NMEs, some finer quantitative and qualitative details are still present in the second-order terms. These corrections include contributions to both the partial half-lives and the β spectra.

Previously, the β decay of ^{113}Cd and ^{115}In were examined in Ref. [8] in the context of the microscopic quasiparticle-phonon model (MQPM) [33] and the NSM [34]. An even earlier study was conducted in Ref. [35]. The considered decay branches are both fourth-forbidden nonunique ground-state-to-ground-state transitions with partial half-lives $t^{\beta}_{1/2} = (8.04 \pm 0.05) \times 10^{15}$ yr and $t^{\beta}_{1/2} = (4.41 \pm 0.25) \times 10^{14}$ yr, respectively [36]. The MQPM is an extension of the QRPA towards the NSM by adding the quasiparticle-phonon coupling to the QRPA to be able to describe the wave functions of odd-mass nuclei. As a result, the features of the QRPA and the NSM propagate to the MQPM, which makes also the MQPM susceptible to the problem of the effective $g_{\rm A}$.

The additional goal of the current work is to further extend the analysis of the mentioned decay branches. This is achieved by expanding the previous MQPM calculations [8] to a larger model space and by performing the nuclear-structure calculations with the microscopic interacting boson-fermion model (IBFM-2) [37,38]. In what follows we denote it as IBM for brevity. The quality of the resulting one-body transition densities (OBTDs) is assessed by examining the spectroscopic properties of the nuclear-structure calculations. After finding a reasonable match with the data, a detailed comparison between the results of the three nuclear models is performed.

The current article is organized as follows. In Sec. II we discuss the theoretical formalism for nuclear β decay in a streamlined manner without resorting to the rigorous derivations of the various mathematical expressions. Special emphasis is placed on the presentation of the second-order terms of the β-decay shape factor in a way to be suitable for practical calculations. In Sec. III we revisit the β decays of ^{113}Cd and ^{115}In by performing an additional study with the IBM wave functions and the presently computed wave functions of MQPM. We compare these results to the ones obtained previously with the NSM. Lastly, in Sec. IV, we draw the conclusions.

II. THEORETICAL FORMALISM

In this section we present the theoretical formalism for nuclear β decay. Although the current presentation follows closely the prescription found in Ref. [1] (see also Ref. [2]), we do not discuss the theory in full detail. Instead of the rigorous derivation of the relevant mathematical expressions, we aim to present the formalism in a compact and ready-to-use way that allows its application to practical calculations. Special care is taken when including the next-to-leading-order terms (or second-order terms) of the β-decay shape function into the equations of the transition half-lives. This refinement of the theory is usually omitted (see, e.g., Ref. [39]).

It should be noted that we focus on the β^- decay, since these are the types of decay examined in the current work. A detailed description on how the presented formalism has to be modified to analyze the β^+ decay branches is reviewed in Sec. II B. An additional discussion on the radiative corrections is briefly made in Sec. II C.

A. Theory of β^- decays

The starting point of the low-energy β^--decay theory is to describe the nuclear β^- decay process with a point-like interaction vertex. The resulting effective coupling constant is then called the Fermi coupling constant $G_{\rm F}$ and the probability for the electron to be emitted in an energy interval W_e to $W + {\rm d}W_e$ is given by

$$P(W_e){\rm d}W_e = \frac{G_{\rm F}^2}{(\hbar c)^6}\frac{1}{2\pi^3\hbar}C(W_e)p_e c W_e(W_0 - W_e)^2 F_0(Z,W_e){\rm d}W_e. \quad (1)$$

The quantity p_e in Eq. (1) is the electron momentum and W_0 is the endpoint energy of the β spectrum. The endpoint energy corresponds to the maximum electron energy in a given transition. The function $F_0(Z,W_e)$ is the Fermi function, and it approximately takes into account the effects of the Coulombic attraction between the electron and the nucleus. Aside from electron energy, the Fermi function is dependent on the proton number Z of the daughter nucleus.

The decay rate associated with a β^- transition is found by integrating Eq. (1) over the accessible energy range of the electron, i.e., from the electron rest mass $m_e c^2$ to the endpoint energy W_0. To treat the integration of this function in a more convenient manner we introduce the dimensionless quantities $w_0 = W_0/(m_e c^2)$, $w_e = W_e/(m_e c^2)$, and $p = p_e c/(m_e c^2) = (w_e^2 - 1)^{1/2}$. These are the corresponding kinematical quantities divided by the electron rest mass $m_e c^2$. By introducing also a constant κ written as

$$\kappa = \frac{2\pi^2\hbar\ln(2)}{(m_e c^2)^5(G_{\rm F}\cos\theta_{\rm C})^2/(\hbar c)^6}, \quad (2)$$

where $\theta_{\rm C}$ is the Cabibbo angle, the partial half-life can then be expressed as $t_{1/2} = \kappa/\tilde{C}$. The quantity $\tilde{C}$ is called the dimensionless integrated shape function and is given by

$$\tilde{C} = \int_1^{w_0} C(w_e)pw_{\rm e}(w_0 - w_e)^2 F_0(Z,w_e)dw_e. \quad (3)$$

Apart from the universal kinematical factors the shape of the β spectrum is determined by the shape factor $C(w_e)$. This is the part that characterizes a given transition by carrying the actual nuclear-structure information in a form of the nuclear matrix elements (NMEs).

The general form of the shape factor of Eq. (3) is a sum:

$$C(w_e) = \sum_{k_e,k_\nu,K}\lambda_{k_e}\left[M_K(k_e,k_\nu)^2 + m_K(k_e,k_\nu)^2 - \frac{2\gamma_{k_e}}{k_e w_e}M_K(k_e,k_\nu)m_K(k_e,k_\nu)\right], \quad (4)$$

where the indices k_e and k_ν (both $k = 1,2,3,...$) are related to the partial-wave expansion of the electron (e) and neutrino (ν) wave functions, and K is the order of forbiddeness of the transition. The Coulomb function λ_{k_e} is given by

$$\lambda_{k_e} = \frac{F_{k_e-1}(Z,W_e)}{F_0(Z,W_e)}, \tag{5}$$

where $F_{k-1}(Z,W_e)$ is the generalized Fermi function which takes the form

$$F_{k_e-1}(Z,W_e) = 4^{k_e-1}(2k_e)\big(k_e+\gamma_{k_e}\big)[(2k_e-1)!!]^2 e^{\pi y} \times \left(\frac{2p_eR}{\hbar}\right)^{2(\gamma_{k_e}-k_e)} \left(\frac{\big|\Gamma\big(\gamma_{k_e}+iy\big)\big|}{\Gamma\big(1+2\gamma_{k_e}\big)}\right)^2. \tag{6}$$

The auxiliary quantities are defined as $\gamma_{k_e} = [k_e^2 - (\alpha Z)^2]^{1/2}$ and $y = (\alpha Z w_e)/(p_e c)$.

The general expressions for the quantities $M_K(k_e,k_\nu)$ and $m_K(k_e,k_\nu)$ are complicated collections of nuclear form factors $\mathcal{F}_{KLS}(q^2) = \mathcal{F}_{KLS}(|p_e + p_\nu|^2)$ and other kinematical factors. Since the most important contributions stem from the form factors that are related to the minimal transfer of angular momentum, Eq. (4) can be restricted to two distinct sums that satisfy $k_e + k_\nu = K + 1$ and $k_e + k_\nu = K + 2$ for a given order of forbiddeness K. These two cases correspond to the angular-momentum transfers ΔJ and $\Delta J + 1$, where $\Delta J = |J_f - J_i|$.

The form factors appearing in Eq. (4) can be expanded as a power series of the quantity $qR/\hbar$, where $q = |p_e + p_\nu|$ and R is the nuclear radius:

$$\mathcal{F}_{KLS}(q^2) = \sum_N \frac{(-1)^N(2L+1)!!}{(2N)!!(2L+2N+1)!!}(qR/\hbar)^{2N}\mathcal{F}^{(N)}_{KLS}. \tag{7}$$

In typical nuclear β decays the momenta of the participating leptons are small, i.e.,

$$(p_eR/\hbar) \ll 1, \quad (p_\nu R/\hbar) \ll 1, \tag{8}$$

where it follows that likewise $(qR/\hbar) \ll 1$. Thus, leading-order contributions come from the lowest-order form-factor coefficients $\mathcal{F}^{(N)}_{KLS}$ of Eq. (7) [1]. In practice the form-factor coefficients are suppressed by a set of small quantities $\eta_{i=1,2,3,4,5} = \{\alpha Z,\ p_eR/\hbar,\ p_\nu R/\hbar,\ m_ecR/\hbar,\ W_eR/\hbar c\}$. When the prefactors dependent on the integers k_e, k_ν, and K are excluded, the functions $M_K(k_e,k_\nu)$ and $m_K(k_e,k_\nu)$, appearing in Eq. (4), consist of terms of the form $\prod_i \eta_i^{\alpha_i}\mathcal{F}^{(N)}_{KLS}$ with $\alpha_i = 0,1,2,....$ Careful and thorough order-of-magnitude considerations are needed to separate the most essential content from the less significant contributions.

To be able to express the nuclear-structure content in a form of NMEs, the decaying nucleus is treated by assuming impulse approximation [1]. The purpose of it is to treat the decaying nucleon independently of the rest of the nucleons. Therefore other nucleons act only as spectators, and the meson-exchange and other many-body effects are neglected. After the impulse approximation is introduced, the nuclear form-factor coefficients can be replaced by

$$R^{LV}F^{(N)}_{KLS}(k_e,m,n,\rho) \to (-1)^{K-L\ V}\mathcal{M}^{(N)}_{KLS}(k_e,m,n,\rho), \tag{9}$$

and

$$R^{LA}F^{(N)}_{KLS}(k_e,m,n,\rho) \to (-1)^{K-L+1\ A}\mathcal{M}^{(N)}_{KLS}(k_e,m,n,\rho). \tag{10}$$

It should be noted that all NMEs carry a prefactor of either $g_{\rm A}$ or $g_{\rm V}$. These are the vector (V) and axial-vector (A) coupling constants that were used to renormalize the hadronic current. The appearance of these constants in Eq. (4) alters the relative weight of NMEs. When the value of $g_{\rm A}$ is increased, the impact of the axial-vector-type NMEs increases. The exact opposite happens when the value is decreased.

Most applications of the β-decay theory (see, e.g., Refs. [5–7,39]) are performed considering only the first-order terms in Eq. (4). The introduction of the next-to-leading-order terms of the shape factor leads to a drastic increase of the number of NMEs involved in the calculations. In the case of fourth-forbidden nonunique decays of the current study, the number of NMEs increases from 12 to 45. In general, second-order terms involve matrix elements that are obtained from the first-order NMEs by adding an extra factor of $(r/R)^{2N}$ to the integrands of the first-order single-particle matrix elements [2]. However, for several terms, the higher-degree Coulombic factors are also taken into account.

Abiding by the dimensionless notation of Eq. (3), the explicit expressions that include both the first- and second-order terms of the shape factor can be constructed as follows: In the case of the summation $k_e + k_\nu = K + 1$ the function $M_K(k_e,k_\nu)$ is given by

$$\begin{aligned}
M_K(k_e,k_\nu) = \mathcal{K}_K\xi^{k_e+k_\nu-2}\big(\sqrt{w_e^2-1}\big)^{k_e-1}(w_0-w_e)^{k_\nu-1}\Bigg[&\sqrt{\frac{2K+1}{K}}R^{-(K-1)}g^V_{\rm V}\mathcal{M}^{(0)}_{K\,K-1\,1} \\
&-\left(\frac{w_e}{2k_e+1}+\frac{w_0-w_e}{2k_\nu+1}\right)\xi R^{-K}g^V_{\rm V}\mathcal{M}^{(0)}_{K\,K\,0} \\
&-\frac{\alpha Z}{2k_e+1}R^{-K}g^V_{\rm V}\mathcal{M}^{(0)}_{K\,K\,0}(k_e,1,1,1)+\sqrt{\frac{K+1}{K}}\left(\frac{w_e}{2k_e+1}-\frac{w_0-w_e}{2k_\nu+1}\right)\xi R^{-K}g^A_{\rm A}\mathcal{M}^{(0)}_{K\,K\,1} \\
&+\sqrt{\frac{K+1}{K}}\frac{\alpha Z}{2k_e+1}R^{-K}g^A_{\rm A}\mathcal{M}^{(0)}_{K\,K\,1}(k_e,1,1,1)-2\sqrt{\frac{K+1}{2K+1}}\frac{w_e}{2k_e+1}\frac{w_0-w_e}{2k_\nu+1}\xi^2R^{-(K+1)}g^V_{\rm V}\mathcal{M}^{(0)}_{K\,K+1\,1} \\
&-2\sqrt{\frac{K+1}{2K+1}}\frac{\alpha Z}{2k_e+1}\frac{w_0-w_e}{2k_\nu+1}\xi R^{-(K+1)}g^V_{\rm V}\mathcal{M}^{(0)}_{K\,K+1\,1}(k_e,1,1,1)
\end{aligned}$$

$$
\begin{aligned}
&+\frac{1}{\sqrt{K(2K+1)}}\frac{w_e}{2k_e+1}\frac{w_0-w_e}{2k_\nu+1}\xi^2 R^{-(K-1)} g_{\rm V}^V \mathcal{M}^{(1)}_{K\,K-1\,1}\\
&+\frac{1}{2}\sqrt{\frac{2K+1}{K}}\left(\frac{1}{2k_e+1}-\frac{w_e^2}{2k_e+1}-\frac{(w_0-w_e)^2}{2k_\nu+1}\right)\xi^2 R^{-(K-1)} g_{\rm V}^V \mathcal{M}^{(1)}_{K\,K-1\,1}\\
&+\frac{1}{\sqrt{K(2K+1)}}\frac{\alpha Z}{2k_e+1}\frac{w_0-w_e}{2k_\nu+1}\xi R^{-(K-1)} g_{\rm V}^V \mathcal{M}^{(1)}_{K\,K-1\,1}(k_e,1,1,1)\\
&-\sqrt{\frac{2K+1}{K}}\frac{\alpha Z w_e}{2k_e+1}\xi R^{-(K-1)} g_{\rm V}^V \mathcal{M}^{(1)}_{K\,K-1\,1}(k_e,2,2,1)\\
&-\frac{1}{2}\sqrt{\frac{2K+1}{K}}\frac{(\alpha Z)^2}{2k_e+1} R^{-(K-1)} g_{\rm V}^V \mathcal{M}^{(1)}_{K\,K-1\,1}(k_e,2,2,2)\Bigg],
\end{aligned}
\tag{11}
$$

and the function $m_K(k_e,k_\nu)$ is given by

$$
\begin{aligned}
m_K(k_e,k_\nu) = \mathcal{K}_K \xi^{k_e+k_\nu-1}\left(\sqrt{w_e^2-1}\right)^{k_e-1}(w_0-w_e)^{k_\nu-1}\frac{1}{2k_e+1}\Bigg[&-R^{-K} g_{\rm V}^V \mathcal{M}^{(0)}_{K\,K\,0}+\sqrt{\frac{K+1}{K}}R^{-K} g_{\rm A}^A \mathcal{M}^{(0)}_{K\,K\,1}\\
&-2\sqrt{\frac{K+1}{2K+1}}\frac{w_0-w_e}{2k_\nu+1}\xi R^{-(K+1)} g_{\rm V}^V \mathcal{M}^{(0)}_{K\,K+1\,1}+\frac{1}{\sqrt{K(2K+1)}}\frac{w_0-w_e}{2k_\nu+1}\xi R^{-(K-1)} g_{\rm V}^V \mathcal{M}^{(1)}_{K\,K-1\,1}\\
&-\frac{1}{2}\sqrt{\frac{2K+1}{K}}\alpha Z R^{-(K-1)} g_{\rm V}^V \mathcal{M}^{(1)}_{K\,K-1\,1}(k_e,2,1,1)\Bigg].
\end{aligned}
\tag{12}
$$

The auxiliary quantity $\xi = m_e c^2 R/(\hbar c)$ and the common prefactor $\mathcal{K}_K$ of both Eqs. (11) and (12) is

$$
\mathcal{K}_K = \sqrt{\frac{1}{2}}\sqrt{\frac{(2K)!!}{(2K+1)!!}}\sqrt{\frac{1}{(2k_e-1)!(2k_\nu-1)!}}.
\tag{13}
$$

The corresponding expressions in the case of the more extensive sum, i.e., $k_e+k_\nu = K+2$, are given by

$$
\begin{aligned}
M_K(k_e,k_\nu) = \tilde{\mathcal{K}}_K \xi^{k_e+k_\nu-2}\left(\sqrt{w_e^2-1}\right)^{k_e-1}(w_0-w_e)^{k_\nu-1}\sqrt{\frac{K+1}{(2k_e-1)(2k_\nu-1)}}\Bigg[&R^{-K} g_{\rm V}^V \mathcal{M}^{(0)}_{K\,K\,0}+\frac{k_e-k_\nu}{\sqrt{K(K+1)}}R^{-K} g_{\rm A}^A \mathcal{M}^{(0)}_{K\,K\,1}\\
&+\sqrt{\frac{1}{(K+1)(2K+1)}}\left(\frac{2k_e-1}{2k_e+1}w_e+\frac{2k_\nu-1}{2k_\nu+1}(w_0-w_e)\right)\xi R^{-(K+1)} g_{\rm V}^V \mathcal{M}^{(0)}_{K\,K+1\,1}\\
&+\sqrt{\frac{1}{(K+1)(2K+1)}}\frac{2k_e-1}{2k_e+1}\alpha Z R^{-(K+1)} g_{\rm V}^V \mathcal{M}^{(0)}_{K\,K+1\,1}(k_e,1,1,1)\\
&+\sqrt{\frac{1}{K(2K+1)}}\left(\frac{2(k_\nu-1)}{2k_e+1}w_e+\frac{2(k_e-1)}{2k_\nu+1}(w_0-w_e)\right)\xi R^{-(K-1)} g_{\rm V}^V \mathcal{M}^{(1)}_{K\,K-1\,1}\\
&+\sqrt{\frac{1}{K(2K+1)}}\frac{2(k_\nu-1)}{2k_e+1}\alpha Z R^{-(K-1)} g_{\rm V}^V \mathcal{M}^{(1)}_{K\,K-1\,1}(k_e,1,1,1)\Bigg],
\end{aligned}
\tag{14}
$$

and

$$
\begin{aligned}
m_K(k_e,k_\nu) = \tilde{\mathcal{K}}_K \xi^{k_e+k_\nu-1}\left(\sqrt{w_e^2-1}\right)^{k_e-1}(w_0-w_e)^{k_\nu-1}&\sqrt{\frac{K+1}{(2k_e+1)(2k_\nu+1)}}\frac{1}{2k_e+1}\\
&\times\left[\sqrt{\frac{1}{(K+1)(2K+1)}}(2k_e-1)R^{-(K+1)} g_{\rm V}^V \mathcal{M}^{(0)}_{K\,K+1\,1}+2\sqrt{\frac{1}{K(2K+1)}}(k_\nu-1)R^{-K} g_{\rm A}^A \mathcal{M}^{(1)}_{K\,K\,1}\right].
\end{aligned}
\tag{15}
$$

It should be noted that, in this case, there are no first-order terms for $m_K(k_e,k_\nu)$. The prefactor $\tilde{\mathcal{K}}_K$ in now expressed as

$$
\tilde{\mathcal{K}}_K = \sqrt{\frac{(2K)!!}{(2K+1)!!}}\sqrt{\frac{1}{(2k_e-1)!(2k_\nu-1)!}}.
\tag{16}
$$

In addition to the terms (14) and (15) the more extensive sum also includes additional terms:

$$
\begin{aligned}
M_{K+1}(k_e,k_\nu) = \tilde{\mathcal{K}}_K \xi^{k_e+k_\nu-2}\left(\sqrt{w_e^2-1}\right)^{k_e-1}(w_0-w_e)^{k_\nu-1}\Bigg[& - R^{-K} g_{\rm A}^A \mathcal{M}^{(0)}_{K+1\,K\,1} \\
& + \sqrt{\frac{K+1}{2K+3}}\left(\frac{w_e}{2k_e+1}+\frac{w_0-w_e}{2k_\nu+1}\right)\xi R^{-(K+1)} g_{\rm A}^A \mathcal{M}^{(0)}_{K+1\,K+1\,0} \\
& + \sqrt{\frac{K+1}{2K+3}}\frac{\alpha Z}{2k_e+1} R^{-(K+1)} g_{\rm A}^A \mathcal{M}^{(0)}_{K+1\,K+1\,0}(k_e,1,1,1) \\
& - \sqrt{\frac{K+2}{2K+3}}\left(\frac{w_e}{2k_e+1}-\frac{w_0-w_e}{2k_\nu+1}\right)\xi R^{-(K+1)} g_{\rm V}^V \mathcal{M}^{(0)}_{K+1\,K+1\,1} \\
& - \sqrt{\frac{K+2}{2K+3}}\frac{\alpha Z}{2k_e+1} R^{-(K+1)} g_{\rm V}^V \mathcal{M}^{(0)}_{K+1\,K+1\,1}(k_e,1,1,1)\Bigg].
\end{aligned}
\tag{17}
$$

The NMEs carry the nuclear-structure information, and for the above equations they are given by the general form

$$
{}^{V/A}\mathcal{M}^{(N)}_{KLS}(pn)(k_e,m,n,\rho) = \frac{\sqrt{4\pi}}{\widehat{J_i}}\sum_{pn}^{V/A} m^{(N)}_{KLS}(pn)(k_e,m,n,\rho)(\Psi_f||[c_p^\dagger \tilde{c}_n]_K||\Psi_i).
\tag{18}
$$

The quantity ${}^{V/A}m^{(N)}_{KLS}(pn)(k_e,m,n,\rho)$ is the single-particle matrix element and the summation of Eq. (18) runs over the proton (p) and neutron (n) single-particle states. The quantity $(\Psi_f||[c_p^\dagger \tilde{c}_n]_K||\Psi_i)$ is the one-body transition density (OBTD) between the initial (i) and final (f) nuclear state, and they must be evaluated by using a given nuclear model. Equation (18) introduces the "hat notation," $\widehat{j} = \sqrt{2j+1}$, which is used throughout Sec. II.

The single-particle matrix elements of Eq. (18) come from sandwiching the β-decay transition operator between the initial (neutron) and final (proton) single particle wave functions, i.e.,

$$
{}^{V}m^{(N)}_{KLS}(pn)(k_e,m,n,\rho) = \frac{1}{\hat{K}}\left(p\left|\left|T_{KLS}\left(\frac{r}{R}\right)^{2N}\mathcal{I}(k_e,m,n,\rho;r)\right|\right|n\right),
\tag{19a}
$$

$$
{}^{A}m^{(N)}_{KLS}(pn)(k_e,m,n,\rho) = \frac{1}{\hat{K}}\left(p\left|\left|\gamma_5 T_{KLS}\left(\frac{r}{R}\right)^{2N}\mathcal{I}(k_e,m,n,\rho;r)\right|\right|n\right),
\tag{19b}
$$

where

$$
T_{KLS} = \begin{cases} i^L r^L Y_{LM}\delta_{LK}, & S=0 \\ i^L(-1)^{L+1-K} r^L [Y_L \boldsymbol{\sigma}]_{KM}, & S=1, \end{cases}
\tag{20}
$$

and γ_5 is the fifth 4×4 gamma matrix with the two off-diagonal 2×2 identity matrices. Functions Y_{LM} are spherical harmonics and $\boldsymbol{\sigma}$ is the Pauli matrix.

In the current work the initial and final states of Eq. (19) are described by the relativistic single-particle spinor wave functions

$$
\phi_{nljm} = \begin{bmatrix} G_{nljm}(\mathbf{r}) \\ F_{nljm}(\mathbf{r}) \end{bmatrix},
\tag{21}
$$

where the large component G_{nljm} is a solution of the nonrelativistic Schrödinger equation for a harmonic oscillator:

$$
G_{nljm}(\mathbf{r}) = i^L g_{nl}(r)[Y_l \chi_{1/2}]_{jm}.
\tag{22}
$$

The small component F_{nljm} is

$$
F_{nljm}(\mathbf{r}) = \frac{\sigma\cdot\mathbf{p}}{2M_{\rm N}c}G_{nljm}(\mathbf{r}) = \frac{i^{l+1}\hbar}{2M_{\rm N}cb}(-1)^{l+j-\frac{1}{2}}\left[\frac{r}{b}g_{nl}(r) - 2\sqrt{n+j+1}\,g_{nl\pm1}(r)\right][Y_{l\pm1}\chi_{1/2}]_{jm}.
\tag{23}
$$

The latter line of Eq. (23) is the analytic form of the smaller component when $g_{nl}(r)$ in taken to be a harmonic-oscillator wave function. The quantity $M_{\rm N} = 940$ MeV$/c$ is the nuclear mass, which is taken to be the same for both protons and neutrons, and b is the harmonic-oscillator size parameter.

All the necessary NMEs required in Eqs. (11)–(17) can be generated from only four types of single-particle matrix element. Depending on the vector or axial-vector character, these types are either ${}^{V/A}m^{(N)}_{KK0}(pn)(k_e,m,n,\rho)$ or ${}^{V/A}m^{(N)}_{KL1}(pn)(k_e,m,n,\rho)$.

The explicit expressions for these elements are

$$
\begin{aligned}
{}^{V}m^{(N)}_{KK0}(pn)(k,m,n,\rho) &= i^{l_p+l_n+K}(-1)^{j_p+j_n+1}\frac{1+(-1)^{l_p+l_n+K}}{2}\frac{\hat{j}_p\hat{j}_n}{\sqrt{4\pi}\hat{K}}\left(j_p\tfrac{1}{2}j_n-\tfrac{1}{2}\middle|K0\right)\\
&\times\frac{1}{R^{2N}}\big[(-1)^{j_n+l_n-\frac{1}{2}}\langle r^{2N+K}\mathcal{I}(k,m,n,\rho;r)\rangle_{pn}\Delta(l_pl_nK)\\
&+(-1)^{j_p+l_p-\frac{1}{2}}\langle r^{2N+K}\mathcal{I}(k,m,n,\rho;r)\rangle_{\tilde{p}\tilde{n}}\Delta(\tilde{l}_p\tilde{l}_nK)\big],
\end{aligned}
\tag{24}
$$

$$
\begin{aligned}
{}^{A}m^{(N)}_{KK0}(pn)(k,m,n,\rho) &= i^{l_p+l_n+K+1}(-1)^{j_p+j_n}\frac{1+(-1)^{l_p+l_n+K+1}}{2}\frac{\hat{j}_p\hat{j}_n}{\sqrt{4\pi}\hat{K}}\left(j_p\tfrac{1}{2}j_n-\tfrac{1}{2}\middle|K0\right)\\
&\times\frac{1}{R^{2N}}[\{r^{2N+K}\mathcal{I}(k,m,n,\rho;r)\}_{p\tilde{n}}\Delta(l_p\tilde{l}_nL)+(-1)^{j_p+j_nl_p+l_n}\{r^{2N+K}\mathcal{I}(k,m,n,\rho;r)\}_{\tilde{p}n}\Delta(\tilde{l}_pl_nL)],
\end{aligned}
\tag{25}
$$

$$
\begin{aligned}
{}^{V}m^{(N)}_{KL1}(pn)(k,m,n,\rho) &= i^{l_p+l_n+L+1}\frac{1+(-1)^{l_p+l_n+L+1}}{2}\frac{\hat{L}\hat{j}_p\hat{j}_n}{\sqrt{4\pi}\hat{K}}\left(j_p\tfrac{1}{2}j_n-\tfrac{1}{2}\middle|K0\right)\\
&\times\frac{1}{R^{2N}}\big[(-1)^{l_n+j_n+\frac{1}{2}+K}[\mathcal{A}_{KL}(pn)+\mathcal{B}_{KL}(pn)]\{r^{2N+K}\mathcal{I}(k,m,n,\rho;r)\}_{p\tilde{n}}\Delta(l_p\tilde{l}_nL)\\
&+(-1)^{l_p+j_p+\frac{1}{2}+K}[\mathcal{A}_{KL}(pn)-\mathcal{B}_{KL}(pn)]\{r^{2N+K}\mathcal{I}(k,m,n,\rho;r)\}_{\tilde{p}n}\Delta(\tilde{l}_pl_nL)\big],
\end{aligned}
\tag{26}
$$

and

$$
\begin{aligned}
{}^{A}m^{(N)}_{KL1}(pn)(k,m,n,\rho) &= i^{l_p+l_n+L}(-1)^{K+1}\frac{1+(-1)^{l_p+l_n+L}}{2}\frac{\hat{L}\hat{j}_p\hat{j}_n}{\sqrt{4\pi}\hat{K}}\left(j_p\tfrac{1}{2}j_n-\tfrac{1}{2}\middle|K0\right)\\
&\times\frac{1}{R^{2N}}[\mathcal{A}_{KL}(pn)+\mathcal{B}_{KL}(pn)]\langle r^{2N+K}\mathcal{I}(k,m,n,\rho;r)\rangle_{pn}\Delta(l_pl_nL)\\
&+(-1)^{l_p+l_n+j_p+j_n}[\mathcal{A}_{KL}(pn)-\mathcal{B}_{KL}(pn)]\{r^{2N+K}\mathcal{I}(k,m,n,\rho;r)\}_{\tilde{p}\tilde{n}}\Delta(\tilde{l}_p\tilde{l}_nL)].
\end{aligned}
\tag{27}
$$

In all the above expression $\Delta(l_1l_2L)$ denotes the triangular condition $|l_1-l_2|\leqslant L\leqslant l_1+l_2$ that the angular-momentum quantum numbers l have to satisfy. If this condition is not met the term vanishes. The auxiliary quantum number $\tilde{l}$, related to the orbital angular-momentum quantum number l, is defined as

$$
\tilde{l}=\begin{cases}l+1, & j=l+\frac{1}{2}\\ l-1, & j=l-\frac{1}{2}.\end{cases}
\tag{28}
$$

In additional to this, the factors $\mathcal{A}_{KL}(pn)$ and $\mathcal{B}_{KL}(pn)$ of Eqs. (26) and (27) are given by

$$
\mathcal{A}_{KL}(pn)=\frac{\hat{j}_p^2+(-1)^{j_p+j_n+K}\hat{j}_n^2}{\sqrt{2K(K+1)(2L+1)}}(-1)^{K+1}(K\,1\,1\,-1|L\,0)(1-\delta_{K0}),
\tag{29}
$$

and

$$
\mathcal{B}_{KL}(pn)=(-1)^{l_p+j_p-\frac{1}{2}+K}\frac{1}{\hat{L}}(K\,0\,1\,0|L\,0).
\tag{30}
$$

The quantities $(j_1\,m_1\;j_2\,m_2|J\;M)$ appearing in Eqs. (24)–(27), (29), and (30), are the usual Clebsch–Gordan coefficients related to the coupling of two angular momenta.

The factors $\{r^{2N+K}\mathcal{I}(k,m,n,\rho;r)\}_{pn}$ of Eqs. (25)–(27), dependent on the radial coordinate r, are called the radial factors, and with the auxiliary notations $\tilde{p}=(n_p,\tilde{l}_p,j_p)$ and $\tilde{n}=(n_n,\tilde{l}_n,j_n)$ they are expressed as

$$
\{r^{2N+K}\mathcal{I}(k,m,n,\rho;r)_{p\tilde{n}}\}=k(b)\left(\frac{1}{b}\langle r^{2N+K+1}\mathcal{I}(k,m,n,\rho;r)\rangle_{pn}-2\sqrt{n_n+j_n+1}\langle r^{2N+K}\mathcal{I}(k,m,n,\rho;r)\rangle_{p\tilde{n}}\right),
\tag{31}
$$

$$
\{r^{2N+K}\mathcal{I}(k,m,n,\rho;r)_{\tilde{p}n}\}=k(b)\left(\frac{1}{b}\langle r^{2N+K+1}\mathcal{I}(k,m,n,\rho;r)\rangle_{pn}-2\sqrt{n_p+j_p+1}\langle r^{2N+K}\mathcal{I}(k,m,n,\rho;r)\rangle_{\tilde{p}n}\right),
\tag{32}
$$

and

$$\{r^{2N+K}\mathcal{I}(k,m,n,\rho;r)_{\tilde{p}\tilde{n}}\} = k(b)^2\left(\frac{1}{b^2}\langle r^{2N+K+2}\mathcal{I}(k,m,n,\rho;r)\rangle_{pn} - \frac{2}{b}\sqrt{n_p+j_p+1}\langle r^{2N+K+1}\mathcal{I}(k,m,n,\rho;r)\rangle_{\tilde{p}n}\right.$$
$$-\frac{2}{b}\sqrt{n_n+j_n+1}\langle r^{2N+K+1}\mathcal{I}(k,m,n,\rho;r)\rangle_{p\tilde{n}}$$
$$\left.+4\sqrt{(n_p+j_p+1)(n_n+j_n+1)}\langle r^{2N+K}\mathcal{I}(k,m,n,\rho;r)\rangle_{\tilde{p}\tilde{n}}\right), \tag{33}$$

where $k(b) = \hbar/(2M_{\mathrm{N}}cb)$. The radial integral itself is defined as

$$\langle r^{2N+L}\mathcal{I}(k,m,n,\rho;r)\rangle_{pn} = \int_0^\infty g_{n_p l_p}(r) r^{2N+L}\mathcal{I}(k,m,n,\rho;r) g_{n_n l_n}(r) r^2 dr, \tag{34}$$

and inside of it are the Coulomb factors $\mathcal{I}(k,m,n,\rho;r)$. These factors take into account the finite size of the nucleus, and they are tabulated by using the integers m, n, and ρ. These are related to the content of the small quantities η_i as follows: m is equal to the total power of $(m_e R/\hbar)$, $(W_e R/\hbar)$ and αZ, n to the total power of $(W_e R/\hbar)$ and αZ, and finally ρ is the power of αZ. If $\rho = 0$ then it always holds that $\mathcal{I}(k,m,n,0;r) = 1$. Thus, the Coulomb factor is explicitly indicated only when it deviates from unity. When the second-order terms are included there is a total of four Coulomb factors involved in the calculations. These are given by

$$\mathcal{I}(k,1,1,1;r) = \begin{cases} \frac{3}{2} - \frac{2k+1}{2(2k+3)}\left(\frac{r}{R}\right)^2 & 0 \leqslant r \leqslant R \\ \frac{2k+1}{2k}\frac{R}{r} - \frac{3}{2k(2k+3)\left(\frac{R}{r}\right)^{2k+1}} & r > R, \end{cases} \tag{35a}$$

$$\mathcal{I}(k,2,1,1;r) = \begin{cases} -\frac{1}{2(2k+3)}\left(\frac{r}{R}\right)^2 & 0 \leqslant r \leqslant R \\ -\frac{1}{k}\frac{R}{r} + \frac{3}{2(2k-1)\left(\frac{R}{r}\right)^2 - \frac{3}{k(2k+3)(2k-1)}\left(\frac{R}{r}\right)^{2k+1}} & r > R, \end{cases} \tag{35b}$$

$$\mathcal{I}(k,2,2,1;r) = \begin{cases} \frac{3}{2} - \frac{k+1}{2(2k+3)}\left(\frac{r}{R}\right)^2 & 0 \leqslant r \leqslant R \\ \frac{4k+1}{2k}\frac{R}{r} - \frac{3k}{2(2k-1)}\left(\frac{R}{r}\right)^2 + \frac{3}{2k(2k+3)-1)}\left(\frac{R}{r}\right)^{2k+1} & r > R, \end{cases} \tag{35c}$$

$$\mathcal{I}(k,2,2,2;r) = \begin{cases} \frac{9}{4} - \frac{3(k+1)}{2(2k+3)}\left(\frac{r}{R}\right)^2 + \frac{2k+1}{12(2k+3)}\left(\frac{r}{R}\right)^4 & 0 \leqslant r \leqslant R \\ \frac{2k+1}{k}\left(\frac{R}{r}\right)^2 \ln\left(\frac{r}{R}\right) + \left[\frac{19}{12} + \frac{7}{12(2k+3)} - \frac{3}{2k^2(2k+3)}\right]\left(\frac{R}{r}\right)^2 + \frac{3}{2k^2(2k+3)\left(\frac{R}{r}\right)^{2k+2}} & r > R, \end{cases} \tag{35d}$$

when uniform charge density is assumed. It should be noted that only the first factor of Eq. (35d) is needed if the shape factor is built from the lowest-order terms.

Further considerations must be taken in the case of the first-forbidden transitions with zero angular-momentum change, i.e., $K = 1$ and $\Delta J = 0$. In this case the shape factor of Eq. (4) is extended by two more nuclear matrix elements to be written in a form

$$C_{01}(w_e) = \xi^2 g_{\mathrm{A}}^2\left[\left(\frac{1}{\xi^2}{}^A\mathcal{M}^{(0)}_{000} + \frac{w_0}{3}{}^A\mathcal{M}^{(0)}_{011} - \frac{\tilde{\alpha}Z}{3}{}^A\mathcal{M}^{(0)}_{011}(k_e,1,1,1)\right)^2 + \left(\frac{{}^A\mathcal{M}^{(0)}_{011}}{3}\right)^2\right.$$
$$\left. - \frac{2\gamma_1}{w_e}\left(\frac{1}{\xi^2}{}^A\mathcal{M}^{(0)}_{000} + \frac{w_0}{3}{}^A\mathcal{M}^{(0)}_{011} - \frac{\tilde{\alpha}Z}{3}{}^A\mathcal{M}^{(0)}_{011}(k_e,1,1,1)\right)\left(\frac{{}^A\mathcal{M}^{(0)}_{011}}{3}\right)\right]. \tag{36}$$

Here $\tilde{\alpha}Z = \frac{\alpha\hbar}{Rm_e c}Z$ and $\gamma_1 = [1-(\alpha Z)^2]^{1/2}$. The auxiliary quantity ξ is the same as in Eqs. (11)–(17). Finally, the new NMEs of the above equation are now expressed as

$${}^A\mathcal{M}^{(0)}_{000} = \frac{\sqrt{4\pi}}{\widehat{J_i}}\sum_{pn}^{A} m^{(0)}_{000}(pn)(\Psi_f||[c_p^\dagger \tilde{c}_n]_0||\Psi_i), \tag{37a}$$

$${}^A\mathcal{M}^{(0)}_{011} = \frac{\sqrt{4\pi}}{\widehat{J_i}}\sum_{pn}^{A} m^{(0)}_{011}(pn)(\Psi_f||[c_p^\dagger \tilde{c}_n]_0||\Psi_i). \tag{37b}$$

The explicit forms of the corresponding single-particle matrix elements can be easily derived from Eqs. (25) and (27).

It is worth emphasizing that the omission of the second-order terms leads to a considerable simplification when dealing

with unique transitions, i.e., those with $\Delta J = K + 1$. In this case only the first term of $M_{K+1}(k_e,k_\nu)$ is nonvanishing in Eq. (4). Therefore, the decay probability is determined solely by a single matrix element ${}^{A}\mathcal{M}^{(0)}_{K+1\,K\,1}$. Furthermore, it follows that the inverse half-life is then proportional to $g_{\rm A}^2$, and thus only one positive value of $g_{\rm A}$ can correspond to the experimentally measured half-life. In contrast to this simplified scheme the inverse half-life for a nonunique decay branch bears the proportionality $1/t_{1/2} \propto c_1 g_{\rm A}^2 + c_2 g_{\rm A} + c_3$, where it generally holds that $c_2 \neq 0$. Due to this nonzero first-power term it follows that a total of two values of $g_{\rm A}$ can reproduce the experimental half-life.

B. β^+ decays

The β^+ decays differ from the β^- decays by the sign of the electric charge of the emitted β particle. Instead of mutual attraction, resulting from the negatively charged electron, the repulsive Coulombic force between the positively charged positron and the daughter nucleus helps to drive the two decay remnants apart. On average, the positrons are emitted at slightly larger energies, and thus the bulk of the β spectrum is shifted to higher energies. Another important difference between the two decay modes comes from the competing electron capture (EC) channel that dominates at low decay energies. The β channel itself is, in fact, available only for energies which are two electron rest masses above the EC threshold.

When the above-derived theoretical formalism of β^- decay is applied to β^+ decays, the signs of some of the parameters are changed. In all equations of Sec. II A one must apply the sign changes $Z \to -Z$ and $g_{\rm A} \to -g_{\rm A}$. In addition, the proton and neutron indices of Eqs. (18) must be exchanged, i.e., $p \leftrightarrow n$. By this conversion the proton single-particle state is on the right side of the transition operator.

C. Radiative corrections

Radiative corrections are a set of higher-order corrections that stem from the finer details of the Coulomb interaction. When only the so-called outer radiative corrections are considered, the treatment is independent of the details of the weak and strong interactions [1]. Since these corrections alter the way the observables depend on electron energy, both the β-decay half-lives and electron spectra are affected.

In practice the radiative corrections are applied by replacing the shape factor $C(w_e)$ of Eq. (4) by

$$C_{\rm R}(w_e) = C(w_e)[1 + \delta_{\rm R}(w_e,Z)]. \tag{38}$$

The correction term $\delta_{\rm R}(w_e,Z)$, generally dependent on both the electron energy w_e and the proton number Z of the daughter nucleus, contains the radiative corrections. The correction factor used in the current article contains the first-order factors taken from Ref. [1]. In this case they are written as

$$\delta_{\rm R}(w_e) = \frac{\alpha}{2\pi} g(w_e,w_0), \tag{39}$$

where

$$\begin{aligned} g(w_e,w_0) = {} & 3\ln\left(\frac{m_p}{m_e}\right) - \frac{3}{4} + 4\left(\frac{\operatorname{arctanh}\beta}{\beta} - 1\right)\frac{w_0 - w_e}{3w_e} \\ & - \frac{3}{2} + \ln[2(w_0 - w_e)] + \frac{4}{\beta}L\left(\frac{2\beta}{1+\beta}\right) \\ & + \frac{\operatorname{arctanh}\beta}{\beta}\left[2(1+\beta^2)\right. \\ & \left. + \frac{(w_0 - w_e)^2}{6w_e^2} - 4\operatorname{arctanh}\beta\right]. \end{aligned} \tag{40}$$

The quantity $\beta = p_e/w_e$ and m_p is the proton mass. The function $L(x)$ appearing in Eq. (40) is the Spence function, defined by the integral

$$L(x) = \int_0^x \frac{dt}{t}\ln(1 - t). \tag{41}$$

It should be noted that the inner radiative corrections, related to the details of the weak and strong interactions, do not change the actual mathematical expressions of the outlined theory. This is because their influence can be absorbed into the renormalization of the weak coupling constants.

III. NUMERICAL APPLICATION AND RESULTS

The application of the theoretical formalism of Sec. II to the highly forbidden β decays is discussed, e.g., in Refs. [3,5–8,35,39]. Previously, the fourth-forbidden nonunique ground-state-to-ground-state decay branches of ^{113}Cd and ^{115}In were examined in Ref. [8]. In that article we introduced a new method for the extraction of the effective values of the weak coupling constants from the β spectra. This method, called the spectrum-shape method (SSM), utilizes the dependence of the shape of the β spectra on the values of the coupling constants. It complements the usual method of extracting the effective values of the weak constants through the inspection of the partial half-lives.

A. Nuclear-structure calculations and β-decay nuclear matrix elements

To further analyze the ^{113}Cd and ^{115}In beta decays, the NSM one-body transition densities of the previous study [8] were adopted. The shell-model OBTDs, as stated in Ref. [8], were computed by using the shell-model code NUSHELLX [40] together with a recently constructed effective jj45pna interaction [42,43]. This interaction is based on the CD-Bonn potential and renormalized by using a perturbative G-matrix

TABLE I. Boson-fermion interaction parameters of the IBFM-2 (in MeV).

Nucleus	Γ_ρ	Λ_ρ	A_ρ
^{113}Cd	0.1	1.15	0.2
^{113}In	0.33		
^{115}In	0.29	0.6	−0.11
^{115}Sn	0.6		0.27

TABLE II. Leading-order and next-to-leading-order nuclear matrix elements (NMEs) of the fourth-forbidden ground-state-to-ground-state decay branches of ^{113}Cd and ^{115}In. The Coulomb-corrected elements [indicated by (k_e,m,n,ρ)] are given when such elements exist.

Transition	^{113}Cd → ^{113}In			^{115}In → ^{115}Sn		
NME	MQPM	NSM	IBM	MQPM	NSM	IBM
$^{V}\mathcal{M}^{(0)}_{K\,K-1\,1}$	0.37093	0	0	0.339021	0	0
$^{V}\mathcal{M}^{(0)}_{K\,K\,0}$	827.136	719.314	316.75	885.423	518.902	218.471
(1,1,1,1)	942.644	824.127	361.636	1014.09	595.72	249.85
(2,1,1,1)	887.642	777.042	340.685	956.052	561.948	235.464
(3,1,1,1)	857.779	751.456	329.307	924.507	543.585	227.646
(4,1,1,1)	839.173	735.502	322.216	904.835	532.129	222.771
$^{A}\mathcal{M}^{(0)}_{K\,K\,1}$	739.05	685.728	274.59	818.152	528.614	194.925
(1,1,1,1)	843.818	787.593	314.226	938.796	609.195	223.324
(2,1,1,1)	794.925	743.029	296.184	885.449	575.183	210.554
(3,1,1,1)	768.365	718.799	286.38	856.439	556.676	203.612
(4,1,1,1)	751.81	703.682	280.268	838.338	545.123	199.281
$^{A}\mathcal{M}^{(0)}_{K+1\,K\,1}$	1231.05	727.205	1345.87	–1449.11	–653.096	975.538
$^{V}\mathcal{M}^{(1)}_{K\,K-1\,1}$	–5.16903	–4.85728	–2.0881	–5.43713	–3.59752	–1.44848
(1,1,1,1)	–4.4566	–4.31234	–1.85226	–4.71801	–3.20201	–1.28761
(2,1,1,1)	–3.88073	–3.79097	–1.6279	–4.11607	–2.8166	–1.1322
(3,1,1,1)	–3.5801	–3.51804	–1.51048	–3.80132	–2.6146	–1.05077
(4,1,1,1)	–3.39941	–3.35355	–1.43972	–3.61185	–2.49273	–1.00165
(1,2,1,1)	–14.2135	–12.6232	–5.43569	–14.904	–9.37363	–3.7838
(2,2,1,1)	–6.89847	–6.12272	–2.63658	–7.23407	–4.5471	–1.83557
(3,2,1,1)	–4.52774	–4.01697	–1.72983	–4.74802	–2.98336	–1.20435
(4,2,1,1)	–3.36423	–2.98388	–1.28497	–3.52783	–2.21612	–0.894638
(1,2,2,1)	–5.51056	–5.26465	–2.26211	–5.8183	–3.90537	–1.57128
(2,2,2,1)	–5.3512	–5.121	–2.20028	–5.65218	–3.79939	–1.52853
(3,2,2,1)	–5.26428	–5.04258	–2.16653	–5.56152	–3.74151	–1.50518
(4,2,2,1)	–5.20989	–4.99348	–2.14539	–5.50477	–3.70526	–1.49056
(1,2,2,2)	–5.87122	–5.72475	–2.45846	–6.22539	–4.25306	–1.70978
(2,2,2,2)	–5.57189	–5.4524	–2.34128	–5.91227	–4.05168	–1.6286
(3,2,2,2)	–5.4081	–5.30326	–2.27712	–5.74085	–3.94136	–1.58414
(4,2,2,2)	–5.30532	–5.2096	–2.23683	–5.63323	–3.87207	–1.55621
$^{V}\mathcal{M}^{(0)}_{K\,K+1\,1}$	1023.51	900.797	387.245	1075.64	675.02	271.785
(1,1,1,1)	1151.5	1016.48	436.79	1212.01	762.778	306.924
(2,1,1,1)	1081.42	955.311	410.461	1138.62	717.089	288.496
(3,1,1,1)	1043.64	922.311	396.259	1099.03	692.427	278.549
(4,1,1,1)	1020.24	901.865	387.46	1074.5	677.138	272.384
$^{A}\mathcal{M}^{(1)}_{K\,K\,1}$	900.171	818.701	331.958	979.65	623.673	234.616
$^{A}\mathcal{M}^{(0)}_{K+1\,K+1\,0}$	–25.2447	–19.9225	0.661943	128.691	–15.6578	1.43613
(1,1,1,1)	–28.1439	–35.2859	0.794223	142.33	–26.7169	2.56177
(2,1,1,1)	–26.3787	–36.0267	0.758084	133.12	–27.1412	2.61864
(3,1,1,1)	–25.4307	–36.3335	0.738638	128.172	–27.3072	2.64266
(4,1,1,1)	–24.8456	–36.4722	0.726605	125.119	–27.3751	2.65384
$^{V}\mathcal{M}^{(0)}_{K+1\,K+1\,1}$	1043.55	736.521	1017.05	–1197.83	–526.737	757.894
(1,1,1,1)	1128.05	802.404	1084.12	–1305.41	–572.825	812.971
(2,1,1,1)	1049.1	747.668	1004.7	–1216.45	–533.488	754.563
(3,1,1,1)	1006.87	718.34	962.338	–1168.78	–512.41	723.351
(4,1,1,1)	980.901	700.279	936.353	–1139.43	–499.429	704.178

approach. The nucleus ^{78}Ni was taken as an inert core, and the orbitals $1p_{3/2}$, $0f_{5/2}$, $1p_{1/2}$, $0g_{9/2}$ and $0g_{7/2}$, $1d_{5/2}$, $1d_{3/2}$, $2s_{1/2}$, $0h_{11/2}$ served as valence spaces for protons and neutrons, respectively. Neutron configurations of these calculations were truncated by allowing no excitations to the $0h_{11/2}$ orbital. For $A = 113$ the orbital $0g_{7/2}$ was forced to be completely filled.

In the case of the MQPM, the OBTDs of Ref. [8] were likewise chosen for the ^{115}In decay. However, a new calculation was performed for ^{113}Cd with an extended neutron valence space [44]. By taking ^{112}Cd as the reference nucleus for ^{113}Cd, the proton valence space was constructed from the orbitals $0f$-$1p$-$0g$-$1d$-$2s$-$0h$, in accordance with Ref. [8]. The new neutron valence space, on the other hand, was built

above the $N = 28$ core including also the $1f$-$2p$ and $0i_{13/2}$ orbitals. By applying the same expanded valence space to the ^{115}In decay the results did not deviate from those of Ref. [8] and thus we adopted the OBTDs of that reference. For each set of calculations, a realistic Bonn one-meson exchange potential was adopted for the nucleon-nucleon interaction. Slight adjustments of the Wood–Saxon single-particle energies were needed to bring the lowest quasi-particle states close to their experimental counterparts. A 3 MeV cutoff energy was introduced to limit the number of QRPA states when coupling the one-quasiparticle states to the two-quasiparticle QRPA phonons.

The IBFM-2 OBTDs of the present work are calculated by using the even-even ^{112}Cd nucleus as core for both ^{113}Cd and ^{113}In, and ^{114}Cd and ^{114}Sn nuclei as cores for ^{115}In and ^{115}Sn, respectively. The parameters for the core Cd nuclei are taken from Ref. [45], and for ^{114}Sn the only needed parameters are $\epsilon = 1.3\,\text{MeV}$, $c_0^{(\nu)} = -0.6\,\text{MeV}$, and $c_4^{(\nu)} = -0.312\,\text{MeV}$. The valence space is chosen to span the $1p_{3/2}$, $0f_{5/2}$, $1p_{1/2}$, $0g_{9/2}$ proton orbitals and the $0g_{7/2}$, $1d_{5/2}$, $1d_{3/2}$, $2s_{1/2}$, and $0h_{11/2}$ neutron orbitals with unperturbed single-particle energies taken from a Woods–Saxon calculation. The boson-fermion interaction parameters are listed in Table I.

When the next-to-leading-order corrections of the shape factor are taken into account there is a total of 45 nuclear matrix elements involved in the computation of a non-unique fourth-forbidden β decay. In the current work we calculated these elements by using the OBTDs from all three nuclear models. The tabulation of these NMEs in Table II shows that, among the nuclear-structure frameworks considered, IBM generally yields the smallest elements (in terms of the absolute value). The only exception is found for the ^{113}Cd decay for which the IBM matrix element ${}^{A}\mathcal{M}^{(0)}_{K+1\,K\,1}$ is actually the largest. Also quite striking is the similarity between the MQPM and NSM NMEs, despite the conceptual difference between the two models in constructing the wave functions. An interesting observation is made when looking at the values of the NME ${}^{V}\mathcal{M}^{(0)}_{K\,K-1\,1}$: In current calculations this NME is nonvanishing only for the MQPM, indicating that the adopted single-particle model space is much larger for the MQPM than for the other two nuclear models.

B. Effective value of g_A and the next-to-leading-order contributions to the shape factor

The comparison between the computed partial half-lives is presented in Fig. 1. Here the half-life is plotted as a function of g_A to illustrate its dependence on the axial-vector coupling. It should be noted that all the nuclear models yield a similar general behavior due to the features of the shape factor itself. As already explained in Ref. [8] (and in Sec. II A) the shape factor for the forbidden nonunique decays is a second-order polynomial in terms of g_A. The consequences of this dependence are the parabola-shaped curves of Fig. 1. If the nuclear model were to completely undershoot the experimental half-life (in that case the theoretical curve would be under the experimental line), no matching results could be found by any adjustment of the value of g_A (and/or g_V).

While the general behavior of the half-life curve is linked to the functional form of Eq. (4), the specific features of it are, however, determined by the actual NMEs. As seen in Fig. 1, the IBM yields in both cases the most wide-spread curve that pushes the crossing points with the experimental half-life band far away from the canonical choice of $g_A = 1.27$. The extracted values of g_A that actually allow the IBM theory to match the experiment are found to be 0.14 and 1.89 for the ^{113}Cd decay and 0.11 and 1.84 for ^{115}In. Effective values such as these would suggest the need for an extreme quenching of the coupling constant. In contrast to the previous study [8], the revised MQPM OBTDs of the ^{113}Cd decay seem to now follow more closely the results of the NSM. The experimental half-life can be reproduced with the values $g_A = 0.63$ and $g_A = 1.29$ which agree well with $g_A = 0.60$ and $g_A = 1.32$ extracted from the NSM curve of Fig. 1.

The contributions coming from the second-order terms of the shape factor were already examined in Ref. [8] in the cases of the MQPM and NSM nuclear models. In general, the contributions to the IBM-based calculations are similar

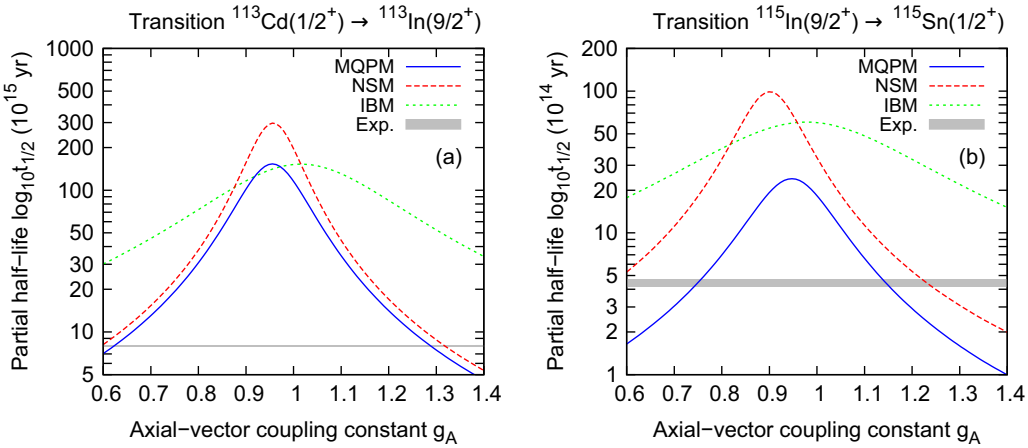

FIG. 1. Partial half-lives of the (a) ^{113}Cd and (b) ^{115}In decay branches as a function of the axial-vector coupling constant g_A. Vector coupling constant is set to $g_V = 1$, and the partial half-lives are calculated up to second order. Experimental half-lives are given as gray horizontal lines.

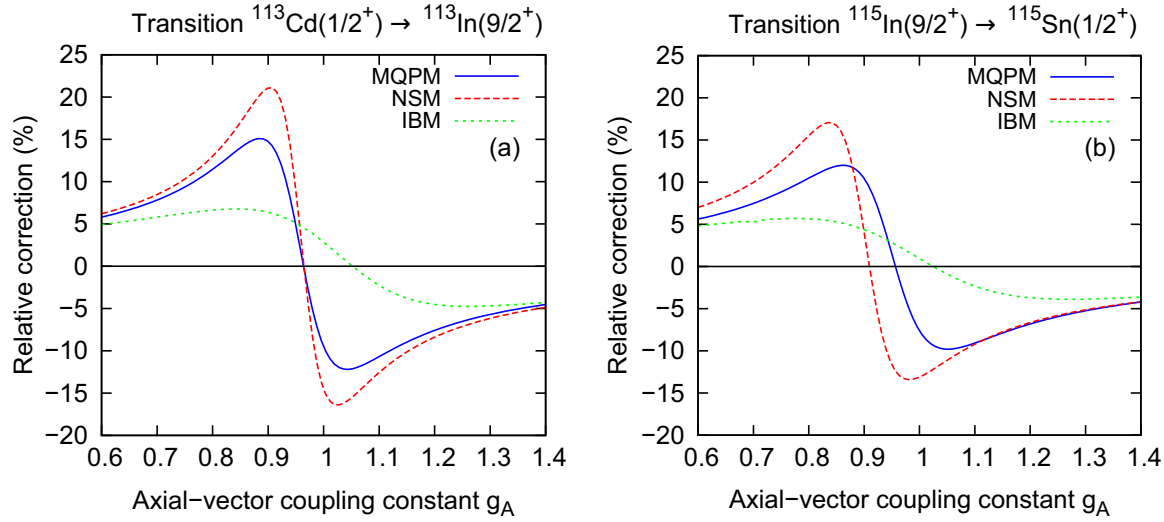

FIG. 2. Dependence of the next-to-leading-order contributions on the axial-vector coupling constant g_A. Graphs represent the relative correction to the partial half-life stemming from the second-order terms of the shape factor.

to contributions to MQPM and NSM. Figure 2 shows that at closer inspection the relative corrections coming from the second-order terms are dependent on the value of g_A. At most these corrections lead to a 20% effect on the partial half-lives in the studied cases. In each case the relative correction changes its sign at g_A close to unity. Thus at low values of the axial-vector coupling the second-order terms push the partial half-life up, while at higher values they reduce the half-life.

A relatively small adjustment of the axial-vector coupling was found to have a strong effect on the spectrum shape in Ref. [8]. This dependence was especially strong in the regions were the half-life curves of Fig. 1 peak. To visually summarize the dependence of the spectrum shape on the value of the axial-vector coupling in the context of IBM-based calculations, we plotted a set of β spectra in Fig. 3. These figures present the integrand of Eq. (3) as a function of the electron energy for different values of g_A. The comparison between the three nuclear models shows that the general behavior is similar for both decays. However, taking a closer look, the IBM spectra are much less sensitive to the changes in g_A than those of MQPM and NSM. Spectra calculated by using the IBM OBTDs preserve the form of a broad central maximum for a much wider range of g_A values.

The corrections stemming from the second-order terms of the shape factor also affect the β spectra. The regions of g_A most sensitive to these contributions are easily anticipated by Fig. 2. Further insight in these contributions is obtained when the values of g_A, for which the second-order terms affect the half-life most strongly, are extracted from Fig. 2 and, subsequently, the corresponding β spectra are plotted in Fig. 4. The effects of the next-to-leading-order terms are most significant at low electron energies. When compared to the leading-order contributions they can introduce a correction of up to 30%. Effects of similar size are also seen in ^{115}In decay. Although these contributions are under control in the theoretical framework, there are important implications to the use of SSM coming from the experimental side. The accurate measurement of the low-energy part of the β spectra is difficult due to the low statistics and high background levels. Thus the spectrum-shape alterations stemming from the next-to-leading-order terms are not easily accessible through the experimental data.

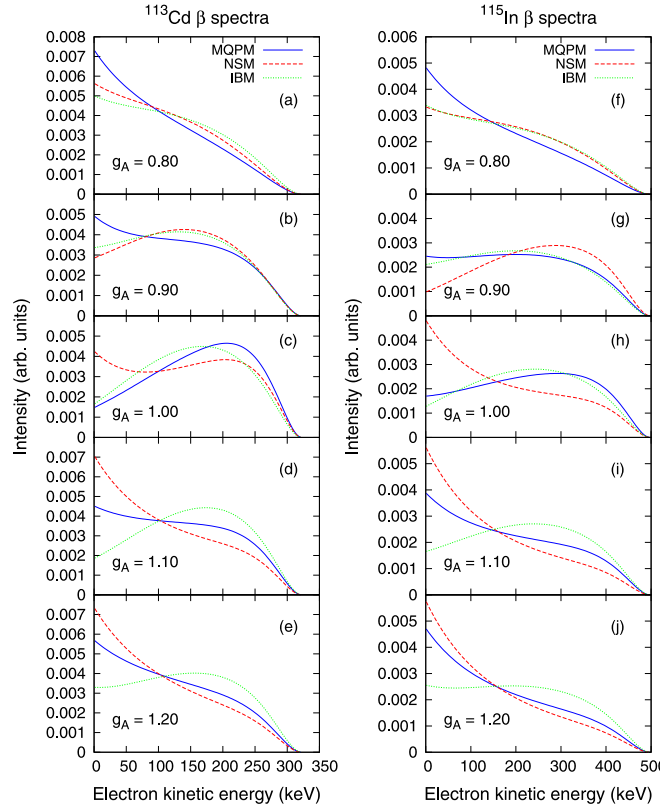

FIG. 3. β spectra of the decays of (a)–(e) ^{113}Cd and (f)–(j) ^{115}In for $g_V = 1.0$. Selected values of the axial-vector coupling are used to illustrate the dependence of the shape of the spectra on the value of g_A. To perform a comparison between the three nuclear models, the areas under each curve are normalized to unity.

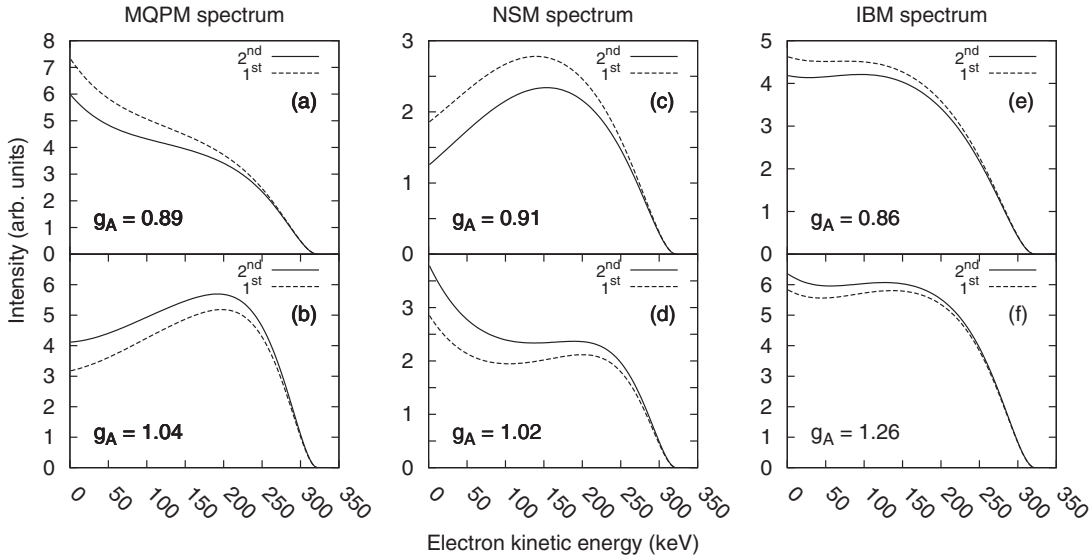

FIG. 4. The extreme effects of the next-to-leading-order terms of the shape factor on the shapes of the β spectra of ^{113}Cd. The adopted values of g_A (indicated in each figure) are extracted from Fig. 2.

Inspection of the effects of the radiative corrections of Eq. (40) shows that these contributions are small. Since there is no explicit dependence of these corrections on the vector or axial-vector coupling, these corrections are fairly constant throughout the range of possible g_A values. The effects on the partial half-lives are less than 2%. The effects on the β spectra are likewise small and of the same order of magnitude. The same conclusion applies also to the β spectra of the ^{115}In decay.

As already pointed out in Ref. [8], the shape factor can be decomposed as $C = g_V^2 C_V + g_A^2 C_A + g_V g_A C_{VA}$. Here the shape factor is regrouped into vector (V), axial-vector (A), and mixed (VA) terms. This decomposition is applied to the β spectra of ^{113}Cd and ^{115}In in Figs. 5 and 6. The decomposed parts of the upper panels are summed in the lower panels by adopting the values $g_V = g_A = 1.0$ to eliminate the scaling effects caused by the weak-interaction constants. Figures 5 and 6 reveal an interesting feature of the studied β decays. The separate components C_V, C_A, and C_{VA} of the integrand (3) are far larger than the total sum, i.e., the actual β spectrum. The destructive interference caused by the negative sign of the mixed term C_{VA} almost perfectly cancels out the contributions that come from C_V and C_A.

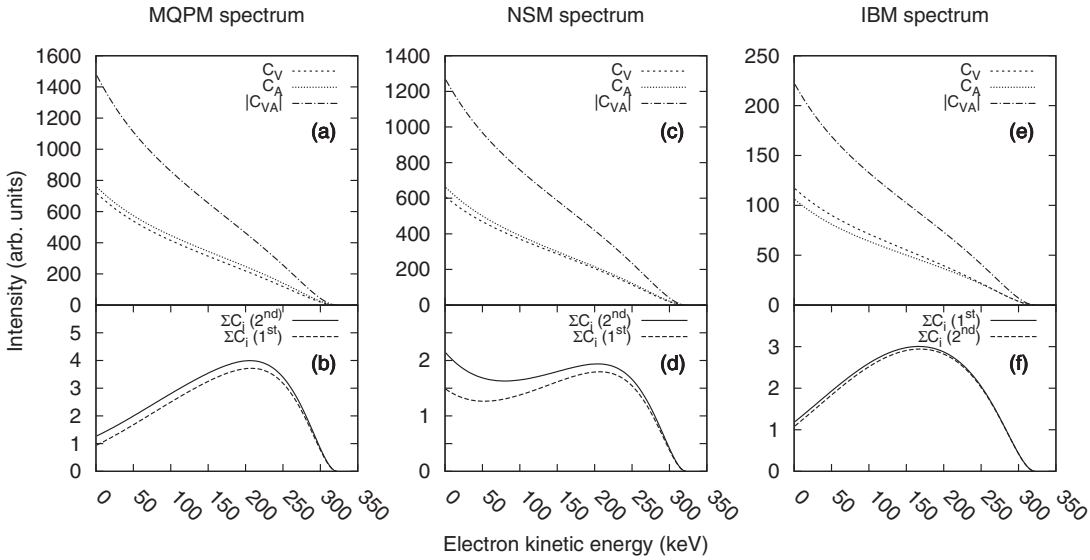

FIG. 5. Decomposed β spectra of the ^{113}Cd decay. In the upper panels the vector (C_V), axial-vector (C_A) and mixed terms (C_{VA}) of the shape factor are presented including the second-order corrections. The lower panels represent the summed β spectra by setting the values of the weak coupling constants to unity. Abbreviation 2nd corresponds to calculations up to second order, and 1st up to first order. The scales on the y axes are chosen to enable an easier visual comparison. Notice that the sign of the mixed term C_{VA} is negative.

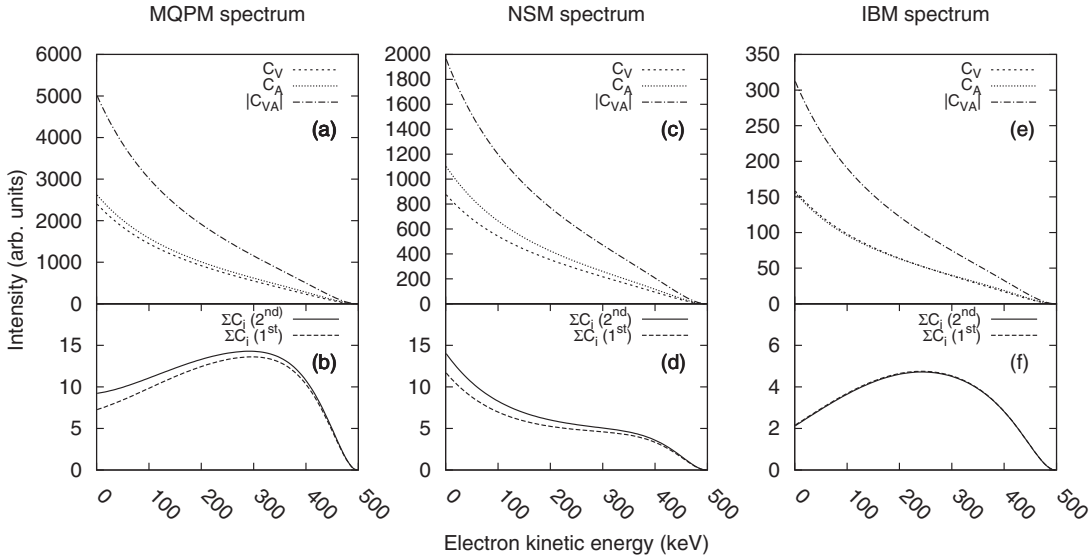

FIG. 6. Decomposed β spectra of the ^{115}In decay (see caption of Fig. 5).

It is worth emphasizing that the observed behavior of both the partial half-lives and β spectra, in terms of $g_{\rm A}$, results from the same source. This is the competition between the vector and axial-vector components. At the point where the partial half-life is at its largest, and at the same time the central maxima of the β spectra most prominent, the relative magnitudes of the terms $g_{\rm V}^2 C_{\rm V}$ and $g_{\rm A}^2 C_{\rm A}$ are reversed. For the low values of $g_{\rm A}$, the vector components dominate over the axial-vector components. For larger values of $g_{\rm A}$ the axial-vector contribution dominates over the vector one.

To summarize the results of our study on the effective values of the axial-vector coupling, we have collected the extracted values of $g_{\rm A}$ in Table III. This includes the results obtained by the use of SSM in the case of ^{113}Cd (see Fig. 7, where the experimental data are taken from Ref. [41]). From Table III one sees that the comparison with the experimental half-lives yields two values of $g_{\rm A}$, which are widely spaced, in particular for the IBM. The results of the SSM are always between these two values in the case of ^{113}Cd decay. The SSM comparison performed in Fig. 7 shows that accurate match with the experiment is found when $g_{\rm A} = 0.93$ for the IBM and $g_{\rm A} = 0.90$ for the NSM. For MQPM an accurate match is not possible to obtain even with the current set of OBTDs, but the best choice would be around $g_{\rm A} = 0.92$. In comparison to Ref. [8], the new value of $g_{\rm A}$ has increased by 0.09, and it now agrees well with the rest of the SSM results. It is thus remarkable that the SSM yields highly consistent results for $g_{\rm A}$, around 0.90–0.93, for all the three nuclear models. However, as already seen in the previous study [8], there is a conflict between the half-life method and the SSM. The

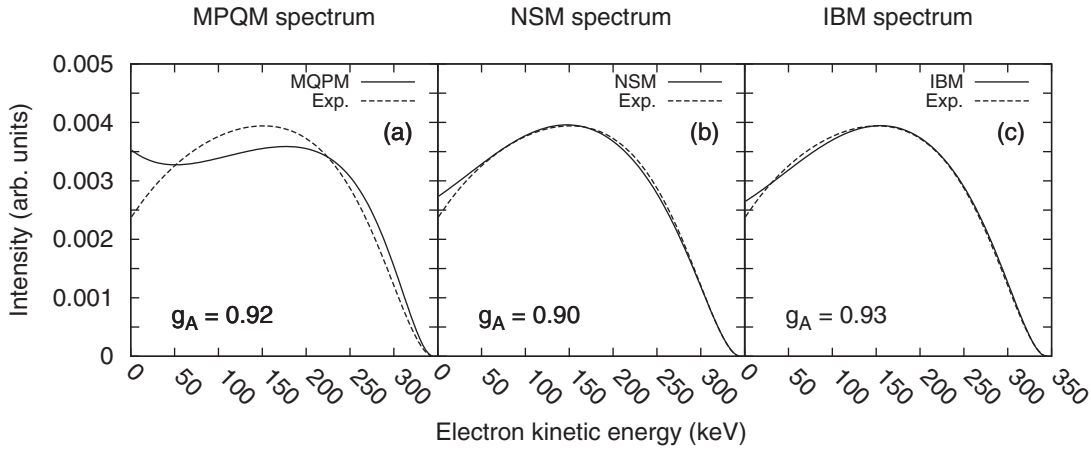

FIG. 7. Comparison of the computed β spectra of ^{113}Cd with the experiment. Computations are done including the second-order corrections, and only the best matches are shown in the figure. The canonical value $g_{\rm V} = 1.0$ is used for the vector coupling constant. Notice that the β-spectrum calculations are done with a Q value of 343.1 ± 0.6 keV to enable comparison with the experimental data of Ref. [41]. The areas under the curves are normalized to unity.

TABLE III. Effective values of g_A extracted by using the partial-half-life method (Half-life) and the spectrum-shape method (SSM). In absence of experimental data, SSM is applied only to the ^{113}Cd decay.

Nuclear model	Effective g_A				
	^{113}Cd			^{115}In	
	Half-life		SSM	Half-life	
MQPM	0.63	1.29	0.92	0.75	1.15
NSM	0.60	1.32	0.90	0.57	1.23
IBM	0.14	1.89	0.93	0.11	1.84

discrepancy seems to be strongly dependent on the available NMEs. This is especially apparent in the case of the IBM-based calculations, where the considered partial half-lives fail to provide any reasonable results for the quenching of g_A. In contrast to this, the half-life results produced by the MQPM and SSM are fairly consistent with each other.

As can be seen, the extracted effective g_A values vary from one theory to the other. Each model used in the present work has its strengths and weaknesses and they propagate to the values extracted for g_A. There is no possibility to trace this propagation quantitatively but, instead, one can list the strengths and weaknesses of the adopted models: The NSM takes into account all the configurations formed from a given single-particle model space, whereas the MQPM and IBM select only the most relevant ones for nuclear low-energy (collective) motion. Both the NSM and IBM suffer from a very restricted size of the single-particle model space, covering essentially one full major shell and leaving out the spin-orbit partners of the model-space orbitals, known to be important for calculation of β-decay and $\beta\beta$-decay properties of nuclei [46]. Contrary to this, the MQPM can handle larger model spaces, including all the spin-orbit partners as in the present work. All these different features reflect in the determination of g_A and could explain the deviations in the results of Table III, in particular concerning the notable deviation of the IBM results from those of the NSM and MQPM.

IV. CONCLUSIONS

In this article we have investigated the fourth-forbidden ground-state-to-ground-state decay branches of ^{113}Cd and ^{115}In and extended the previous analysis of Ref. [8] by displaying the exact expressions of the next-to-leading-order and radiative corrections, as well as including the results obtained by the use of the interacting boson model (IBM) (IBFM-2, to be exact). We have performed a comparison between the results of the three nuclear models and have taken a closer look at the contributions that rise from the next-to-leading-order terms of the β-decay shape function. This additional study was mostly motivated by the introduction of the spectrum shape method (SSM) in Ref. [8]. The beginning of the current article was dedicated to presentation of the theoretical formalism used to handle the nuclear β decay. This was done in a compact and ready-to-use way to allow its application to practical computation of nuclear β-decay half-lives and β spectra.

The results of the current study strengthen the conclusions made in Ref. [8] about the significance of the next-to-leading-order terms of the shape factor. However, while the effects stemming from the second-order terms are generally small, a strong dependence on the value of g_A can be found in closer scrutiny. At best the second-order terms contribute more than 20% to the partial half-life. The effects on the β spectrum shape are harder to quantify, but generally the contributions are most significant at low electron energies. In the region of g_A where the partial half-lives are most affected, the effects on the β spectra can amount to as much as 30%.

The comparison between the results of the three adopted nuclear models, the nuclear shell model (NSM), the IBM, and the microscopic quasiparticle-phonon model (MQPM), points to a tension between the decay-half-life method and the SSM. In the case of the IBM calculations the decay-half-life method seems to fail in providing any reasonable effective values of g_A. While the results obtained by the use of the decay-half-life method vary much from one nuclear model to the other, the results obtained by the use of the SSM are quite consistent, around 0.90–0.93. The IBM-derived value, $g_A = 0.93$, is surprisingly close to both the MQPM and NSM values, $g_A = 0.92$ and $g_A = 0.90$, respectively, considering the very different results obtained in the half-life calculations. It is reasonable to expect that the SSM and the half-life method should produce consistent results when accurate NMEs are used. Thus, the apparent conflict between the SSM and the partial-half-life method seems to point to the direction of defective nuclear matrix elements. To investigate this aspect of the calculations, and to further test the power of the SSM, more studies in different nuclear-structure frameworks and more experimental data on electron β spectra are called for.

As a last point we want to mention the potential application of the present beta-decay formalism to solve, at least partly, the "spectral anomaly" of reactor antineutrino spectra [47]. The antineutrino spectra in the nuclear reactors result from the (long) α and β^- decay chains of the uranium and plutonium nuclei used as fuel of the power plants. The spectral anomaly refers to the deviation of the measured antineutrino spectra, obtained in the large on-going neutrino experiments, from the reference spectra [48] deduced from nuclear data with some approximations. The involved beta decays contain forbidden transitions that cannot be accessed by the present nuclear data, but instead could be calculated by the formalism of the present work. Such considerations we leave for the future.

ACKNOWLEDGMENTS

This work was supported by the Academy of Finland (Suomen Akatemia) under the Finnish Center of Excellence Program 2012-2017 (Nuclear and Accelerator Based Program at JYFL) and Project No. 266437. We want to thank J. Kostensalo for providing us with the new sets of MQPM one-body transitions densities for the ^{113}Cd and ^{115}In decays.

[1] H. Behrens and W. Bühring, *Electron Radial Wave Functions and Nuclear Beta-Decay* (Clarendon Press, Oxford, 1982).
[2] H. F. Schopper, *Weak Interactions and Nuclear Beta Decay* (North-Holland, Amsterdam, 1966).
[3] H. Heiskanen, M. T. Mustonen, and J. Suhonen, J. Phys. G: Nucl. Part. Phys. **34**, 837 (2013).
[4] J. S. E. Wieslander *et al.*, Phys. Rev. Lett. **103**, 122501 (2009).
[5] M. Haaranen and J. Suhonen, Eur. Phys. J. A **49**, 93 (2013).
[6] M. Haaranen, M. Horoi, and J. Suhonen, Phys. Rev. C **89**, 034315 (2014).
[7] M. Haaranen, P. C. Srivastava, J. Suhonen, and K. Zuber, Phys. Rev. C **90**, 044314 (2014).
[8] M. Haaranen, P. C. Srivastava, and J. Suhonen, Phys. Rev. C **93**, 034308 (2016).
[9] M. Alanssari, D. Frekers, T. Eronen, L. Canete, J. Dilling, M. Haaranen, J. Hakala, M. Holl, M. Jeskovsky, A. Jokinen, A. Kankainen, J. Koponen, A. J. Mayer, I. D. Moore, D. A. Nesterenko, I. Pohjalainen, P. Povinec, J. Reinikainen, S. Rinta-Antila, P. C. Srivastava, J. Suhonen, R. I. Thompson, A. Voss, and M. E. Wieser, Phys. Rev. Lett. **116**, 072501 (2016).
[10] M. Märkisch and H. Abele, arXiv:1410.4220.
[11] E. D. Commins, *Weak Interactions* (McGraw-Hill, New York, 1973).
[12] A. Bohr and B. R. Mottelson, Phys. Lett. B **100**, 10 (1981).
[13] J. Suhonen, *From Nucleons to Nucleus: Concepts of Microscopic Nuclear Theory* (Springer, Berlin, 2007).
[14] J. Suhonen and O. Civitarese, Phys. Lett. B **725**, 153 (2013).
[15] J. Suhonen and O. Civitarese, Nucl. Phys. A **924**, 1 (2014).
[16] E. K. Warburton, Phys. Rev. C **42**, 2479 (1990).
[17] E. K. Warburton, Phys. Rev. C **44**, 233 (1991).
[18] T. Suzuki, T. Yoshida, T. Kajino, and T. Otsuka, Phys. Rev. C **85**, 015802 (2012).
[19] Q. Zhi, E. Caurier, J. J. Cuenca-Garcí a, K. Langanke, G. Martínez-Pinedo, and K. Sieja, Phys. Rev. C **87**, 025803 (2013).
[20] J. Suhonen and O. Civitarese, Phys. Rep. **300**, 123 (1998).
[21] J. Maalampi and J. Suhonen, Adv. High Energy Phys. **2013**, 505874 (2013).
[22] H. Ejiri, N. Soukouti, and J. Suhonen, Phys. Lett. B **729**, 27 (2014).
[23] H. Ejiri and J. Suhonen, J. Phys. G: Nucl. Part. Phys. **42**, 055201 (2015).
[24] A. Faessler, G. L. Fogli, E. Lisi, V. Rodin, A. M. Rotunno, and F. Šimkovic, J. Phys. G: Nucl. Part. Phys **35**, 075104 (2008).
[25] D. S. Delion and J. Suhonen, Eur. Phys. Lett. **107**, 52001 (2014).
[26] P. Pirinen and J. Suhonen, Phys. Rev. C **91**, 054309 (2015).
[27] B. H. Wildenthal, M. S. Curtin, and B. A. Brown, Phys. Rev. C **28**, 1343 (1983).
[28] G. Martínez-Pinedo, A. Poves, E. Caurier, and A. P. Zuker, Phys. Rev. C **53**, R2602(R) (1996).
[29] E. Caurier, F. Nowacki, and A. Poves, Phys. Lett. B **711**, 62 (2012).
[30] J. Barea, J. Kotila, and F. Iachello, Phys. Rev. C **87**, 014315 (2013).
[31] J. Barea, J. Kotila, and F. Iachello, Phys. Rev. C **91**, 034304 (2015).
[32] N. Yoshida and F. Iachello, Prog. Theor. Exp. Phys. **2013**, 043D01 (2013).
[33] J. Toivanen and J. Suhonen, Phys. Rev. C **57**, 1237 (1998).
[34] K. L. G. Heyde, *The Nuclear Shell Model* (Springer, Berlin, 1990).
[35] M. T. Mustonen and J. Suhonen, Phys. Lett. B **657**, 38 (2007).
[36] ENSDF at NNDC site: http://www.nndc.bnl.gov/.
[37] F. Iachello and A. Arima, *The Interacting Boson Model* (Cambridge University Press, Great Britain, 1987).
[38] F. Iachello and P. Van Isacker, *The Interacting Boson-Fermion Model* (Cambridge University Press, USA, 1991).
[39] M. T. Mustonen, M. Aunola, and J. Suhonen, Phys. Rev. C **73**, 054301 (2006).
[40] B. A. Brown, W. D. M. Rae, E. McDonald, and M. Horoi, NuShellX@MSU, http://www.nscl.msu.edu/~brown/resources/resources.html.
[41] P. Belli, R. Bernabei, N. Bukilic, F. Cappella, R. Cerulli, C. J. Dai, F. A. Danevich, J. R. deLaeter, A. Incicchitti, V. V. Kobychev, S. S. Nagorny, S. Nisi, F. Nozzoli, D. V. Poda, D. Prosperi, V. I. Tretyak, and S. S. Yurchenko, Phys. Rev. C **76**, 064603 (2007).
[42] R. Machleidt, Phys. Rev. C **63**, 024001 (2001).
[43] S. Lalkovski *et al.*, Phys. Rev. C **87**, 034308 (2013).
[44] J. Kostensalo (private communication).
[45] A. Giannatiempo, A. Nannini, A. Perego, P. Sona, and G. Maino, Phys. Rev. C **44**, 1508 (1991).
[46] J. Suhonen and O. Civitarese, Nucl. Phys. A **847**, 207 (2010).
[47] C. Buck, A. P. Collin, J. Haser, and M. Lindner, Phys. Lett. B **765**, 159 (2017).
[48] T. A. Mueller, D. Lhuillier, M. Fallot, A. Letourneau, S. Cormon, M. Fechner, L. Giot, T. Lasserre, J. Martino, G. Mention, A. Porta, and F. Yermia, Phys. Rev. C **83**, 054615 (2011).